Chemical Effects of Methyl and Methyl Ester Groups on the Nucleation and Growth of Vapor-Deposited Aluminum Films

A. Hooper,[†] G. L. Fisher,[†] K. Konstadinidis,[‡] D. Jung,[†,⊥] H. Nguyen,[§] R. Opila,*[,‡] R. W. Collins,*[,§] N. Winograd,*[,†] and D. L. Allara*[,†]

Contribution from the Departments of Chemistry and Physics, The Pennsylvania State University, University Park, Pennsylvania 16802 and Bell Labs, Lucent Technologies, 600 Mountain Avenue, Murray Hill, New Jersey 07974

Received October 5, 1998

Abstract: The interaction of vapor-deposited Al atoms with self-assembled monolayers (SAMs) of $HS(CH_2)_{15}$-CH_3 and $HS(CH_2)_{15}CO_2CH_3$ chemisorbed at Au{111} surfaces was studied using X-ray photoelectron spectroscopy, infrared spectroscopy, time-of-flight secondary ion mass spectrometry, and spectroscopic ellipsometry. For the CH_3-terminated SAM, no reaction with C−H or C−C bonds was observed. For total Al doses up to ∼12 atoms/nm^2, penetration to the Au−S interface occurs with no disruption of the average chain conformation and tilt, indicating formation of a highly uniform ∼1:1 Al adlayer on the Au. Subsequently, penetration ceases and a metallic overlayer begins to form at the SAM−vacuum interface. These results are explained in terms of an initial dynamic hopping of the −S headgroups on the Au lattice, which opens transient diffusion channels to the Au−S interface, and the closing of these channels upon completion of the adlayer. In contrast, Al atom interactions with the CO_2CH_3-terminated SAM are restricted to the vacuum interface, where in the initial stages discrete organometallic products form via reaction with the CO_2CH_3 group. First, a 1:1 complex forms with a reduced C═O bond and an intact CH_3 moiety. Further exposure leads to the additional reaction of about four Al atoms per ester, after which a metallic overlayer nucleates in the form of clusters. After the growth progresses to ∼30 Å, the clusters coalesce into a uniform metallic film. These results illustrate the extraordinary degree of control that organic substrates can exert during the course of metal film formation.

1. Introduction

The deposition of metal atoms onto the surfaces of organic materials has become a common technological process, particularly for polymers.[1,2] Typically, chemical functionalities at the surface, such as −OH and C═O, serve to activate the polymer toward chemical interactions with the deposited metal. These interactions can produce favorable properties, e.g., strong metal−polymer adhesion. It has been shown that the relative abilities of different surface functional groups to activate chemical vapor deposition[3] can be utilized to generate sharp metal line patterns on chemically patterned substrates.[4] In the area of organic electronic devices, the chemical nature of deposited metal−organic contacts is critical to device performance, e.g., polymer light-emitting diodes.[5] Of particular interest to us has been the fabrication of electronic devices based on surface assemblies of discrete, conjugated organic molecules.[6] In cases requiring a top metal contact,[7] deposition of the metal at the vacuum termini of the molecules requires a delicate balance between establishing metal−organic chemical bonding with appropriate interface electronic states and avoiding chemical degradation of the functional parts of the molecules. In all these applications, an improved understanding of the fundamental nature of metal atom−organic group interactions is desirable.

The need to study the metal/organic interface under carefully controlled conditions has inspired recent studies[8] based on the use of the well-defined surfaces of self-assembled monolayers

[†] Department of Chemistry, The Pennsylvania State University.
[§] Department of Physics, The Pennsylvania State University.
[‡] Bell Labs, Lucent Technologies.
[⊥] Present address: Cellomics, Inc., Pittsburgh, PA 15238.

(1) (a) *Metallized Plastics 5 & 6: Fundamental and Applied Aspects*; Mittal, K. L., Ed.; VSP International Science Publishers: The Netherlands, 1998 (and earlier volumes). (b) *Metallized plastics: fundamentals and applications*; Mittal, K. L., Ed.; Marcel Dekker: New York, 1998. (c) Sacher, E. In *Metallization of Polymers*; Sacher, E., Kowalczyk, S. P., Pireaux, J.-J., Eds.; ACS Symposium Series 440; American Chemical Society: Washington, DC, 1990; pp 1−7. (d) Ho, P. S.; Haight, R.; White, R. C.; Silverman, B. D.; Faupel, F. In *Fundamentals of Adhesion*; Lee, L. H., Ed.; Plenum Press: New York, 1990; pp 383−406. (e) Dannetun, P.; Lögdlund, M.; Fahlman, M.; Boman, M.; Stafström, S.; Salaneck, W. R. *Synth. Met.* **1993**, *55*−*57*, 212−217. (f) Lazzaroni, R.; Brédas, J. L.; Dannetun, P.; Fredriksson, C.; Stafström, S.; Salaneck, W. R. *Electrochim. Acta* **1994**, *39*, 235−244.

(2) Margolis, J. M., Ed. *Conductive polymers and plastics*; Chapman and Hall: New York and London, 1989.

(3) Jeon, N. L.; Nuzzo, R. G. *Langmuir* **1995**, *11*, 341−355.

(4) (a) Jeon, N. L.; Clem, P. G.; Payne, D. A.; Nuzzo, R. G. *Langmuir* **1996**, *12*, 5350−5355. (b) Jeon, N. L.; Nuzzo, R. G.; Xia, Y.; Mrksich, M.; Whitesides, G. M. *Langmuir* **1995**, *11*, 3024−3026.

(5) For example, see: *Conjugated Polymer Surfaces and Interfaces, Electronic and Chemical Nature of Interfaces for Polymer Light Emitting Devices*; Salanek, W. R., Stafstrom, S., Bredas, J.-L., Eds.; Cambridge University Press: Cambridge, UK, 1996.

(6) For example see: *Molecular Electronics*; Aviram, A., Ratner, M., Eds. *Ann. NY. Acad. Sci*. **1998**, *852*, special issue devoted to recent developments in this area.

(7) For example, see: Zhou, C.; Deshpande, M. A.; Reed, M. A.; Jones, L.; Tour, J. M. *Appl. Phys. Lett.* **1997**, *71*, 611−613.

(8) For a review of recent work, see: (a) Jung, D. R.; Czanderna, A. W.; Herdt, G. C. In *Polymer Surfaces and Interfaces: Characterization, Modification and Applications*; Mittal, K. I., Lee, K. W., Eds.; VSP International Science Publishers: The Netherlands, 1997; pp 189−224. (b) Jung, D. R.; Czanderna, A. W. *Crit. Rev. Solid State Mater. Sci.* **1994**, *19*, 1−54.

10.1021/ja9835234 CCC: $18.00
Published on Web 08/18/1999

(SAMs). These monolayers can provide controlled quantities, types, and orientations of organic groups exposed at the vacuum interface.[9−11] This situation is in contrast to typical polymer surfaces, where these properties are rarely controlled or characterized. Quantitative studies with SAM surfaces should be useful not only for improving metalization processes but also for addressing important fundamental questions about organometallic interactions and bonding states that might otherwise be inaccessible by traditional chemical approaches. To achieve such answers, complementary surface science tools are required in order to obtain a thorough, microscopic picture of the atomic and molecular interactions relevant to each interface of interest.

Aluminum deposition onto organic surfaces is of considerable importance to a number of applications, especially in microelectronics,[1] and a variety of studies have been carried out on the interactions of Al with O-containing polymer surfaces.[12] From a more fundamental point of view, Al is a strongly electropositive metal that displays rich organometallic chemistry, especially including compounds with O-containing ligands.[13] The use of closely controlled conditions involving a pristine, well-defined organic surface allows quantitative analysis of product stoichiometries. The $-C(=O)-OCH_3$ group was chosen for this study since it is a typical functional unit in technologically important polymers, e.g., poly(methyl methacrylate) [PMMA] and poly(ethylene terpthalate), and the component C=O group is generally accepted as the key chemically active unit in promoting Al interactions at a variety of polymer surfaces, such as polyimides.[12a−g] Other workers have proposed that Al atoms form various Al−O−C bridged complexes at O-containing polymer surfaces, but details remain sparse. For example, electron energy loss spectroscopy data for Al on polyimide have been interpreted in terms of the formation of an Al complex with the carbonyl sites in the polymer.[12d] Akhter, Zhou, and White[12k,l] have studied the interaction of $(CH_3)_3Al$ on poly(vinyl alcohol) and concluded that triangular Al−O−C complexes form with stoichiometries ranging from 1:1:1 to 1:1.5:1, respectively. On the basis of molecular orbital calculations, Chakraborty, Davis, and Tirrell[14] have proposed that Al atoms interact with the C=O unit of the $-CO_2CH_3$ group of PMMA by electron transfer to the C atom, subsequent complexation with the O atom, and eventual formation of a σ-bonded Al−O−C complex.

In this paper we examine both the structural and dynamical aspects of the interaction of Al atoms with $-CH_3$ and $-CO_2CH_3$ groups on ω-functionalized alkanethiolate SAMs on Au. The Al−organic interactions are examined in situ using high-resolution X-ray photoelectron spectrometry (XPS), infrared reflectance spectroscopy (IRS), time-of-flight secondary ion mass spectroscopy (ToF-SIMS), and spectroscopic ellipsometry (SE) in the near-infrared to ultraviolet regions. Of special interest is to unravel the movement of Al atoms at the surface, since this movement allows competition for binding sites, nucleation of metallic phases, surface chemical reactions, interior diffusion (penetration) into the organic matrix, and reactions at the organic/substrate interface. These issues have been particularly problematic in earlier studies.[8b] Our results show that the $-CO_2CH_3$ group is sufficiently reactive toward Al atoms so as to block both the penetration and overlayer metallic phase nucleation channels. Discrete organometallic complexes, with intact CH_3 units, are formed in the initial deposition stages, ranging from 1:1 stoichiometries at low Al coverages up to a limit of ∼4:1. Further addition of Al results exclusively in the nucleation of metallic clusters at the vacuum interface. In contrast, the chemically inert character of the alkyl chains allows the opening of a dynamic channel, in which Al atoms diffuse to the S−Au interface to form a relatively uniform layer with the striking characteristic of an intact alkyl chain organization. This process is complete after formation of an approximately 1-atom-thick layer, and the deposition shifts to nucleation and growth of a metallic overlayer at the vacuum interface. These results demonstrate how the character of the final metal−organic interface depends critically upon the subtle interplay between the detailed structural characteristics of the organic film, the chemical reactivity of the functional groups present, and metal atom nucleation dynamics.

2. Experimental Section

Self-assembled alkanethiolate monolayers of $-S(CH_2)_{15}CO_2CH_3$ and $-S(CH_2)_{15}CH_3$ on Au-coated Si wafers were prepared and characterized according to previously published procedures.[15] Briefly, self-assembly was carried out in 1 mM ethanol solutions for 4 days. After being thoroughly rinsed with ethanol and acetone, the samples were characterized immediately by IRS, single-wavelength ellipsometry, and liquid drop contact angles. For convenience, the monolayers are designated as **ME-Au** and **M-Au**, respectively.

Four different chambers were used, one for each diagnostic technique. All experiments were performed in situ, with the sample held continuously under vacuum. Aluminum (99.999%) was thermally evaporated from tungsten baskets, with the exception of a boronitride crucible Knudsen cell used for XPS experiments. Deposition rates were maintained at or below 0.5 Å/min for the different techniques, with the exception of the SE experiment, which used a continuous deposition rate of ∼1 Å/s. In the case of the XPS and ToF-SIMS experiments, incremental depositions were done in a fore chamber whose pressure remained below 1×10^{-7} Torr. After deposition, the sample was transferred through a load-lock into the analysis chamber whose pressure remained, in both cases, at $\sim(1-2) \times 10^{-9}$ Torr. In the IR and SE experiments, depositions and analyses were accomplished in a fixed sample configuration. The IR depositions were incremental, with pressures remaining below 1×10^{-7} Torr during deposition and recovering to $\sim 2 \times 10^{-8}$ Torr during analysis. The SE measurements were performed in real time, with spectra taken during deposition.

(9) (a) Ulman, A. *An Introduction to Ultrathin Organic Films, From Langmuir−Blodgett to Self-Assembly*; Academic Press: Boston, 1991. (b) Ulman, A. *Chem. Rev.* **1996**, *96*, 1533−1554.

(10) Dubois, L. H.; Nuzzo, R. G. *Annu. Rev. Phys. Chem.* **1992**, *43*, 437−463.

(11) Zhang, P.; Konstadinidis, P.; Opila, R. L.; Allara, D. L. *Surf. Sci.* **1995**, *338*, 300−312.

(12) Polyimides: (a) Atanasoska, Lj.; Anderson, S. G.; Meyer, H. M., III; Zhangda, L.; Weaver, J. H. *J. Vac. Sci. Technol. A* **1987**, *5*, 3325−3333. (b) Bartha, J. W.; Hahn, P. O.; LeGoues, F.; Ho, P. S. *J. Vac. Sci. Technol. A* **1985**, *3*, 1390−1393. (c) Ho, P. S.; Hahn, P. O.; Bartha, J. W.; Rubloff, G. W.; LeGoues, F. K. *J. Vac. Sci. Technol. A* **1985**, *3*, 739−745. (d) Pireaux, J. J.; Vermeersch, M.; Grégoire, C.; Thiry, P. A.; Caudano, R. *J. Chem. Phys.* **1988**, *88*, 3353−3362. (e) Vasile, M. J.; Bachman, B. J. *J. Vac. Sci. Technol. A* **1989**, *7*, 2992−2997. (f) Domingue, A.; Dignard-Bailey, L.; Sacher, E.; Yelon, A.; Ellis, T. H. In *Metallization of Polymers*; Sacher, E., Kowalczyk, S. P., Pireaux, J.-J., Eds.; ACS Symposium Series 440; American Chemical Society: Washington, DC, 1990; pp 272−287. (g) Selmani, A. In *Metallization of Polymers*; Sacher, E., Kowalczyk, S. P., Pireaux, J.-J., Eds.; ACS Symposium Series 440; American Chemical Society: Washington, DC, 1990; pp 345−351. Poly(acrylic acid): (h) Dekoven, B. M.; Hagans, P. L. *Appl. Surf. Sci.* **1986**, *27*, 199−213. Poly(ethylene terephthalate): (i) Bou, M.; Martin, J. M.; Le Mogne, Th. *Appl. Surf. Sci.* **1991**, *47*, 149−161. Polythiophene: (j) Lazzaroni, R.; Brédas, J. L.; Dannetun, P.; Lögdlund, M.; Uvdal, K.; Salaneck,W. R. *Synth. Met.* **1991**, *41−43*, 3323−3328. Poly(vinyl alcohol): (k) Akhter, S.; Zhou, X.-L.; White, J. M. *Appl. Surf. Sci.* **1989**, *37*, 201−216. (l) Stoyanov, P.; Akhter, S.; White, J. M. *Surf. Interface Anal.* **1990**, *15*, 509−515.

(13) For example, see: *Advances in Organometallic Chemistry*; Stone, F. G., West, R., Eds.; Academic Press: New York, 1996; Vol. 39. *Organometallic Chemistry*; Abel, E. W., Ed.; The Royal Society of Chemistry: Cambridge, UK, 1996; Vol. 25 and earlier volumes.

(14) Chakraborty, A. K.; Davis, H. T.; Tirrell, M. *J. Polym. Sci.* **1990**, *28*, 3185−3219.

(15) Nuzzo, R. G.; Dubois, L. H.; Allara, D. L. *J .Am. Chem. Soc*. **1990**, *112*, 558−569.

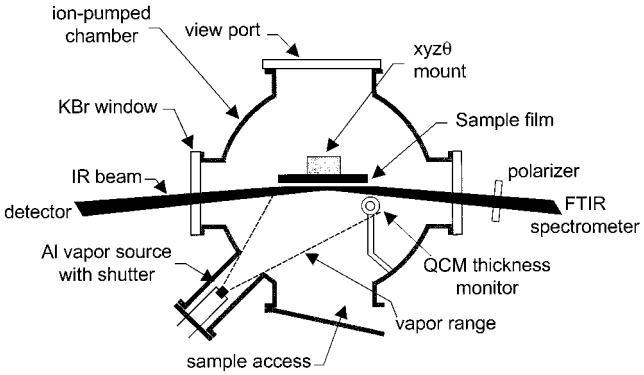

Figure 1. Diagram of the infrared spectrometer interfaced to a vacuum deposition chamber. The polarized IR beam enters and exits the chamber through differentially pumped KBr windows and is incident on the sample at 86°. The Al vapor flux, controlled by a shutter, is monitored by a quartz crystal microbalance thickness monitor.

Throughout the SE runs, the pressure remained at $\sim 5 \times 10^{-8}$ Torr. Thus, for all four probes, the pressure during deposition remained in the 10^{-8} Torr region. Thereafter, all pressures were at that level or lower. As demonstrated by the self-consistency of the results from all the techniques (see later sections), the small discrepancies between the different operating pressures appear to have negligible effects on the courses of the depositions. Aluminum thickness determinations in the IRS and ToF-SIMS chambers were made using precalibrated quartz crystal thickness monitors set near the samples. In the XPS experiments, the thickness was determined by noting the exposure times for each dose, counting the total aluminum on the sample by Rutherford backscattering after removal, and applying the calculated source rate (constant at constant source current) with the dose times. For SE, the deposited film thicknesses were evaluated directly from the SE data. For all the methods, the substrate temperatures were kept within 10 °C of room temperature during the depositions.

Details of the XPS instrument[16,17] and experimental procedure[11] have been published previously. A pass energy of 75 eV and an energy step of 0.05 eV resulted in a full width at half-maximum of 0.52 eV for the Au $4f_{7/2}$ core-level peak. Two sets of samples were employed to determine the sensitivity of the samples to secondary electron damage[18,19] under the analysis conditions. The first received sequential 0.5-, 1-, 2-, and 4-Å Al doses and then was removed. The second received 4-, 8-, and 16-Å doses. Comparison of the two 4-Å-coated samples gave similar results within experimental error, indicating that the longer X-ray exposure condition was not damaging relative to the shortest one. In addition, a SAM was exposed to the X-ray beam overnight. Comparison of the C 1s region before and after X-ray exposure indicated negligible damage.

The IRS spectra were recorded using a Fourier transform instrument (Mattson Research Series, Mattson-ATI, Madison, WI) interfaced via custom optics to a vacuum chamber with differentially pumped KBr windows. A *p*-polarized beam was utilized at an 86° angle of incidence. The optics and spectral details are similar to those utilized for an ambient system reported previously.[20] A manual shutter controlled the Al flux exposure. Data collection after each Al dose took approximately 4 min. Since the details of the vacuum apparatus have not been published previously, a schematic is given in Figure 1.

The ToF-SIMS analysis was performed on a custom-designed instrument.[21] The instrument consists of a load-lock, a preparation chamber, and the primary analysis chamber, each separated by a gate valve. The primary ions are delivered using a Ga^+ liquid metal ion gun (LMIG). The primary ion beam is accelerated to 25 keV and has a probe diameter of 100 nm. The secondary ions are focused into a flight tube by an extraction lens, drift through a field-free region and into a two-stage reflectron where they are time compressed, drift through a second field-free region, and strike the multichannel plate (MCP) detector. During data acquisition, the beam is pulsed with a width of 40 ns at ≤ 2 nA and is rastered over a 1600×1600 μm^2 area. All spectra were acquired using a total ion dose less than 10^{11} ions/cm^2. Under these conditions, the relative peak intensities were reproducible to $\pm 6\%$ from sample to sample and $\pm 6\%$ from scan to scan. Aluminum deposition was carried out in the preparation chamber, using a W wire basket source, at a rate of 0.1 Å/s. Deposition measurements were made using a Sycon STM-100 QCM controller. The maximum error within the Al deposition measurements is $\pm 8\%$.

The SE spectra were obtained on a custom-built multichannel instrument utilizing a rotating (12.5 Hz) polarizer for incident polarization state modulation and a fixed analyzer, followed by a photodiode array connected to a prism spectrograph for reflected polarization state detection.[22] The optical system was interfaced to a deposition chamber. The angle of incidence was set at 70°, and the analyzer was oriented at 30° with respect to the plane of incidence. The array pixels were grouped to provide 83 spectral positions in the ellipsometric angles (ψ, Δ), spanning photon energies from 1.3 to 4.0 eV. The (ψ, Δ) spectra were collected over 0.16 s as an average of four optical cycles (or two full polarizer rotations) during film deposition. The repetition period between successive spectra was 0.94 s. Details of the ellipsometer, including rotating polarizer calibration, data reduction, and error corrections, can be found elsewhere.[23,24]

3. Results

3.1. Overview. The results are presented in terms of those obtained for each characterization technique in the order of XPS, IRS, ToF-SIMS, and SE. In the Discussion section, the data are interrelated, and overall conclusions are drawn about the deposition processes for each type of monolayer film. For the XPS, IRS, and ToF-SIMS experiments, where the total amount of Al delivered to the sample was measured directly, the average dose is given in terms of the hypothetical thickness, d_{Al}, which would be obtained if a uniform film were to form with the density of the bulk metal.

3.2. X-ray Photoelectron Spectroscopy. The C and O 1s core-level shifts for untreated **M-Au** and **ME-Au** collected at both 90 and 10° takeoff angles (10° = near grazing) are in agreement with previous data.[11]

The effects of depositing incremental amounts of Al onto **M-Au** are shown in Figure 2. The C 1s peak at 285 eV diminishes in intensity and becomes broader with increasing d_{Al}, as shown in Figure 2a. The peak shifts to higher binding energy at $d_{Al} = 1$ Å and gradually shifts back to lower binding energy at $d_{Al} = 2$ Å. Such shifting has been noted in a previous study[25] but not explained. The absence of new C 1s peaks indicates that no chemical reaction occurs between Al and the SAM. In particular, the formation of aluminum carbide (expected at 282.3 eV[26]) is not observed. This result is consistent with the earlier work of Jung and Czanderna.[8a] The gradual

(16) Gelius, U.; Wannberg, B.; Baltzer, P.; Fellner-Feldergg, H.; Carlsson, G.; Johansson, C. G.; Larsson, J.; Munger, P.; Vegerfors, G. *J. Electron Spectrosc. Relat. Phenom.* **1990**, *52*, 747−785.

(17) Beamson, G.; Briggs, D.; Davies, S. F.; Fletcher, I. W.; Clark, D. T.; Howard, J.; Gelius, U.; Wannberg, B.; Balzer, P. *Surf. Interface Anal.* **1990**, *15*, 541−549.

(18) Frydman, E.; Cohen, H.; Maoz, R.; Sagiv, J. *Langmuir* **1997**, *13*, 5089−5106.

(19) Wirde, M.; Gelius, U.; Dunbar, T.; Allara, D. L. *Nuclear Instrum. and Methods Phys. Res. B* **1997**, *130*, 1−8.

(20) Parikh, A. N.; Allara, D. L. *J. Chem. Phys.* **1992**, *96*, 927−945.

(21) Braun, R. M.; Blenkinsopp, P.; Mullock, J.; Corlett, C.; Willey, K. F.; Vickerman, J. C.; Winograd, N. *Rapid. Commun. Mass Spectrom.*, in press.

(22) Collins, R. W. *Rev. Sci. Instrum.* **1990**, *61*, 2029−2062.

(23) Nguyen, N. V.; Pudliner, B. S.; An, I.; Collins, R. W. *J. Opt. Soc. Am. A* **1991**, *8*, 919−931.

(24) An, I.; Cong, Y.; Nguyen, N. V.; Pudliner, B. S.; Collins, R. W. *Thin Solid Films* **1991**, *206*, 300−311.

(25) Herdt, G. C.; Czanderna, A. W. *J. Vac. Sci. Technol. A* **1995**, *13*, 1275−1280.

(26) Zhang, P. Study of the Chemistry and the Morphology at the Interface Between Metals and Polymers by Spectroscopic Techniques. Ph.D. Thesis, Penn State University, 1993.

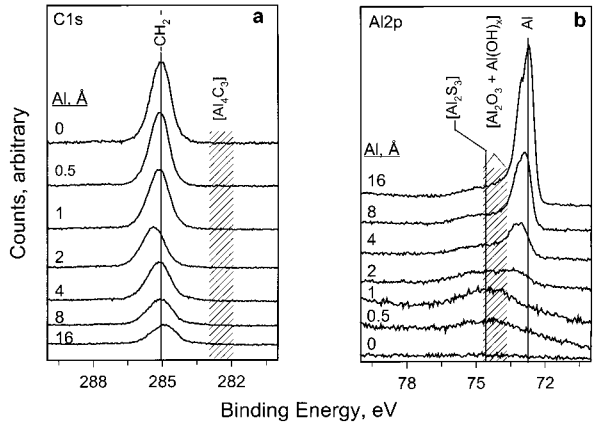

Figure 2. XPS C 1s and Al 2p core-level shifts for the methyl-terminated SAM at different total doses of Al. For reference, typical binding energy regions, where aluminum carbide, sulfide, oxide, and hydroxide species have been reported, are indicated by the location of the bracketed species. The nonbracketed species indicate peak assignments.

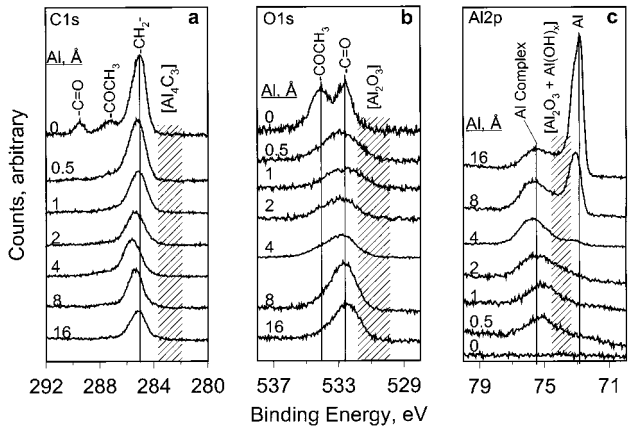

Figure 3. XPS C 1s, O 1s, and Al 2p core-level shifts for the methyl ester-terminated SAM at different total doses of Al. For reference, typical binding energy regions, where aluminum carbide, oxide, and hydroxide species have been reported, are indicated by the location of the bracketed species. The nonbracketed species indicate peak assignments.

losses observed in the alkyl chain signal intensity in our experiments can be straightforwardly attributed to signal attenuation from the growing Al overlayer. The Al 2p core-level spectra in Figure 2b show that a single broad peak at ~74.2 eV is observed at $d_{Al} = 0.5$ Å. Likely sources of this peak would be an Al−O or an Al−S species. Typical binding energies of aluminum oxide,[27,28] hydroxide, and sulfide species[28] are shown in Figure 2. An oxide or hydroxide could arise from reaction of Al with adventitious O_2 or H_2O. An Al−S species would arise from reaction with the thiolate unit. The Al 2p peak for Al_2S_3 occurs at 74.6 eV, while reaction between evaporated Al and the S atoms in polythiophene has been reported[12j] to give an Al 2p feature at ~76 eV. The simplest mechanism for formation of an Al−S species in our experiment is Al atom penetration to the Al/SAM interface. Figure 2b shows that the ~74.2 eV peak begins to diminish past this point. In concert, the C 1s peak clearly shows the onset of attenuation. These changes are consistent with an initial ~1−2 Å accumulation of Al at the Au−S interface,[29] with a shift thereafter to accumulation at the vacuum/SAM surface. In contrast, if the ~74.2 eV peak were due to aluminum oxide (or hydroxide), one would expect that Al was depositing only at the vacuum surface, where reaction with background O-containing species would continually occur with increasing coverage. Eventually, the appearance of a feature at ~73.3 eV after $d_{Al} = 2$ Å indicates the onset of Al metal [Al(0) state] deposition. At higher coverages, the peak shifts further to 72.8 eV. This behavior suggests that the Al metal forms initially as small clusters, which grow larger with continued deposition. The resultant Fermi level shifts would give rise to the binding energy trend. At $d_{Al} = 4$ Å, the metallic Al peak begins to dominate the spectra. The peak at ~74.2 eV is still observed but does not increase with increasing d_{Al}.

(27) Waner, C. D.; Powell, C. J.; Allison, J. W.; Rumble, J. R., Jr.; Blakeslee, D. M.; Dal-Favero, M. E. *NIST X-ray Photoelectron Spectroscopy Database*; U.S. Department of Commerce: Gaithersburg, MD, 1997.

(28) Moulder, J. F.; Stickle, W. F.; Sobol, P. E.; Bomben, K. D. In *Handbook of X-ray Photoelectron Spectroscopy*; Chastain, J., Ed.; Perkin-Elmer Corp.: Eden Prairie, MN, 1992.

(29) An attempt was made to confirm the presence of an $Al_xS_yAu_z$ interfacial species by analysis of the Au 4f and S 2p and core-level regions. The strong Au 4f peaks showed no discernible asymmetry, as expected from the inability to detect any Au−S asymmetry effects in the pure alkanethiolate SAMs. For S, the small 2p photoionization cross section combined with attenuation from the 2 nm organic overlayer results in such weak peaks that the long collection times needed for good signal/noise make the spectra susceptible to X-ray damage artifacts (see ref 19).

The results of analogous experiments performed on **ME-Au** are shown in Figure 3. The peak assignments for the pure SAM spectrum have been reported previously.[11] The C 1s core-level features are shown in Figure 3a. The main peak at 285 eV corresponds to the alkyl chain carbons; the side peaks at 289 and 287 eV in the initial spectrum correspond to the C═O and $-OCH_3$ groups, respectively. At $d_{Al} = 0.5-1$ Å, these side peaks vanish, but otherwise no change is observed. This observation could occur because of reaction of the CO_2CH_3 unit and/or photoelectron attenuation effects of an overlayer of Al. Simple inspection of the spectra shows that the intensities of the *C*═O and *C*−OCH_3 peaks decrease much faster than does the *C*−H intensity. On this basis, it is clear that the former intensities are being reduced by chemical reaction of the functional groups, although the nature of the products is not revealed in the spectra. The O 1s peaks of the $-OCH_3$ and C═O groups appear at 534.1 and 532.6 eV, respectively, as seen in Figure 3b. After $d_{Al} = 0.5$ Å, both peaks are replaced by a single broad peak at 532.9 eV. This behavior implies that there is a significant perturbation of the ester group. Further analysis of these data is complicated by the formation of what appears to be an aluminum oxide, presumably arising from reactions with O_2 and/or H_2O background gases, and by attenuation of the signal intensity by the Al overlayer. Figure 3c shows the Al 2p core-level spectra. Note that, after $d_{Al} = 0.5$ Å, a broad peak, centered at ~75.2 eV, appears. This result contrasts with that found for the **M-Au** SAM, where a broad peak at ~74.2 eV (attributed to an Al−S species) appears at $d_{Al} = 0.5$ Å. The feature in the **ME-Au** SAM appears at a higher binding energy than expected for aluminum oxide. On this basis, we assign the new peak to an Al−O−C species formed from the reaction between Al and the $-CO_2CH_3$ group. Another contrasting result is the appearance of an Al(0) peak (at 72.9 eV) between $d_{Al} =$ 4 and 8 Å on **ME-Au**. On **M-Au**, this species appears between 2 and 4 Å. The delay in the formation of Al(0) would be expected if the Al atoms were reacting with the $-CO_2CH_3$ group to form an Al−C−O species. After $d_{Al} = 8$ Å, the observed increasing dominance of the Al(0) peak in the spectra indicates that a metallic overlayer of Al is accumulating.

3.3. Infrared Spectroscopy. The mode assignments of the spectra of the monolayers have been reported elsewhere.[15] Previous characterization has shown for both monolayers that

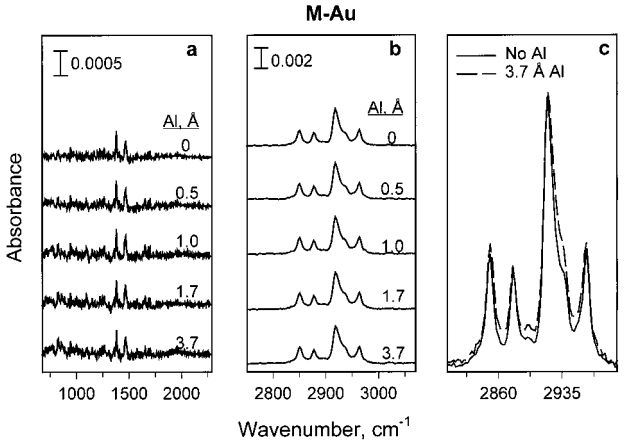

Figure 4. IRS spectra of the methyl-terminated SAM for different total doses of Al. The peak frequencies (in cm^{-1}) and the mode assignments for the initial (no Al) SAM are the following: 2965, CH_3 C−H asym str; 2958, CH_3, C−H asym str; 2938, CH_3, C−H sym str; 2918, CH_2, C−H antisym str; 2878, CH_3, C−H sym str; 2851, CH_2, C−H sym str; 1468, CH_2 scissors def; 1383, CH_3 sym def. Plot c shows an expanded scale overlay of the initial spectrum and that after 3.7 Å deposition of Al.

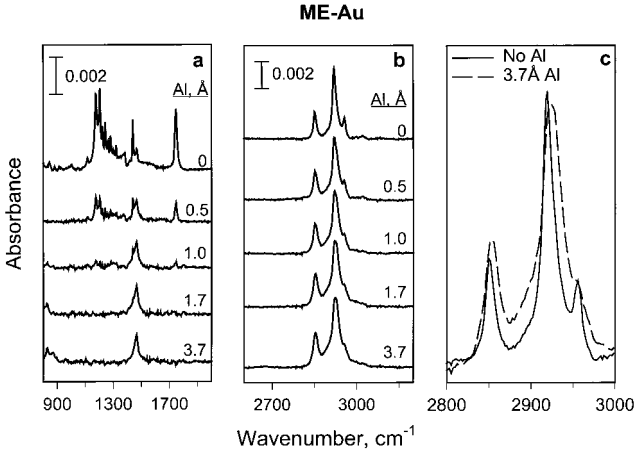

Figure 5. IRS spectra of the methyl ester-terminated SAM at different total doses of Al. The peak frequencies (in cm^{-1}) and the mode assignments for the initial (no Al) SAM are the following: 2955, CH_3 C−H asym str; 2918, CH_2, CH antisym str; 2851, CH_2, C−H sym str; 1746, C═O str; 1465, CH_2, scissors def; 1440, CH_3 sym def; 1150−1350, chain wags and twists (progression bands); 1206, C−O str; 1177, C−O str. Plot c shows an expanded scale overlay of the initial spectrum and that after 3.7 Å deposition of Al.

the chains are in highly trans conformations, with the long axes tilted from the surface normal at an average angle of ∼25−35°.[10,15,20]

The **M-Au** spectra are presented in Figure 4. The major observation is that deposition of Al causes only small perturbations in the spectra; all major features remain, even after ∼4 Å of Al. This observation demonstrates, in agreement with the XPS result, that no chemical interaction occurs between Al and the monolayer. A more detailed examination, however, does reveal a slight broadening in the d^- mode feature at 2918 cm^{-1} upon Al deposition. This behavior suggests the appearance of a correspondingly slight amount of chain disordering. The changes in the high-frequency modes are highlighted in Figure 4c, where the initial spectrum is superimposed on a spectrum taken at $d_{Al} = 2.6$ Å.

In contrast, several major changes are observed with Al deposition on **ME-Au**. In the low-frequency region of the spectrum, shown in Figure 5, one can note that, as d_{Al} increases, evenly distributed intensity losses occur for those mode peaks associated uniquely with the presence of a terminal −C(═O)−OCH_3 group. Of particular importance are the peaks at 1746, 1206, 1177, and 1200−1350 cm^{-1}, assigned, respectively, to the C═O stretch ($\nu_{C=O}$), the C−O stretches (ν_{C-O} and ν^2_{C-O}), and the chain twist-wag modes (ω_{CH_2}). While the ω_{CH_2} modes arise from coupled vibrations of the $-(CH_2)-$ chain, they are unique to the ester group in the sense that their intensities are greatly enhanced when an ester group is attached at the chain terminus (compare this region for Figures 4 and 5).[15] The spectra in Figure 5 show that, by $d_{Al} = 1.0-1.2$ Å, all the ester-related features vanish. In contrast, those features associated with the alkyl chain, independent of the presence of a terminal ester group, show much smaller changes. The CH_2 scissors deformation mode (γ_{CH_2}) peak at 1468 cm^{-1} is virtually unchanged except for a small increase in intensity. The CH_3 symmetric deformation (γ_{CH_3}) peak at 1440 cm^{-1} shows a modest drop in intensity and some broadening. These observations lead to the conclusion that the alkanethiolate chains remain on the surface after Al deposition but the ester group is chemically altered. Further, the changes in the ester group do not involve loss of the CH_3 moiety. Finally, note that a broad peak appears between 800 and 1000 cm^{-1} for $d_{Al} > 2.7$ Å. This feature is reminiscent of the aluminum oxide LO phonon[30] (ν_{Al-O}) of the native oxide on Al metal; accordingly, this feature is assigned to an aluminum oxide species. Using calibrations of the LO-phonon cross section from Al_2O_3/Al samples, we estimate that the observed ν_{Al-O} peak in Figure 5 for $d_{Al} = 3.7$ Å is equivalent to an ∼1 Å layer of aluminum oxide.

In the high-frequency region, all C−H stretching mode peaks remain after Al deposition but undergo noticeable broadening. The d^- mode also shows a significant shift of ∼+5 cm^{-1}. These results indicate that the chains remain on the surface but are conformationally disordered by the Al atoms. This disordering effect is much stronger than that for **M-Au**. It is important to note that, while the CH_3 asymmetric stretching mode (r^-) associated with the O−CH_3 unit (initially at 2955 cm^{-1}) shows a significant broadening, the overall intensity and frequency position remain reasonably constant. This result is consistent with the loss of integrity of the $-CO_2CH_3$ group, but with the constraint that the CH_3 remains chemically intact and bound at the surface. Given the general insensitivity of the r^- mode frequency with respect to bonding to O or Al,[31] it is not possible from the spectra to conclude the final chemical state of the CH_3 group in the reaction product, e.g., O−CH_3 or Al−CH_3. The changes in the high-frequency C−H stretching modes between the initial spectrum and one taken at $d_{Al} = 2.6$ Å are revealed in detail in Figures 4 and 5. Comparison of the high-frequency overlaps in Figures 4 and 5 clearly shows that the changes are greater for the **ME-Au** film than for the **M-Au** film. This behavior shows that there is a much greater perturbation of chain conformational ordering for Al deposition on the **ME-Au** film.

Using the peak intensities of modes associated uniquely with the $-CO_2CH_3$ group, the progress of the reaction of Al atoms with this group can be followed. To do this quantitatively, the selected mode features were isolated by curve-fitting and the

(30) Mertens, F. P. *Surf. Sci.* **1978**, *71*, 161−173.

(31) Possible fates of the CH_3 unit in the Al−CO_2CH_3 system include formation of Al−CH_3 and Al−OCH_3 bonds. Relevant to this, the r^- mode frequency for $Al(CH_3)_3$ is 2958 cm^{-1} (Crompton, T. R. *Comprehensive Organometallic Analysis*; Plenum Press: New York, 1987; Chapter 4), very near the value of 2955 cm^{-1} for the CO_2CH_3 group. While IR data for CH_3O−Al compounds do not appear to be available, the analogous compound $B(OCH_3)_3$ is reported to exhibit r^- at 2955 cm^{-1} (Lehmann, W. J.; Onak, T. P.; Shapiro, I. *J. Chem. Phys.* **1959**, *30*, 1215−1218).

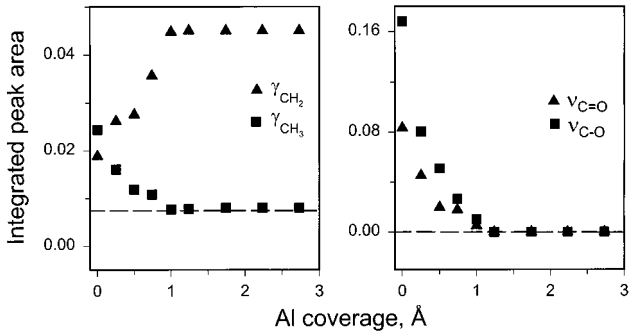

Figure 6. Plots of the changes in selected IRS integrated peak areas of a methyl ester-terminated SAM with total Al coverage in Å. For analysis of the ν_{C-O} features, the areas of both contributing modes were combined.

peak areas determined. The results are given in Figure 6. The ν_{C-O} and ν^2_{C-O} mode intensities decrease until they are completely gone by $d_{Al} \approx 1$ Å. The γ_{CH_3} intensity also decreases but does not vanish. Changes in both the γ_{CH_2} and γ_{CH_3} modes are complete by $d_{Al} \approx 1$ Å. The γ_{CH_3} intensity has more than doubled, while that of the γ_{CH_3} mode is reduced to about one-third of the original value.

All of the above data suggest that the deposited Al atoms cause chemical changes in the $-CO_2CH_3$ group, which in turn induces significant conformational disordering of the alkyl chains. However, note that, although the modes associated with the ester group have disappeared, no new peaks associated with the reaction products are obvious. The only new peak observed is the aluminum oxide phonon in the 800−1000 cm^{-1} region, and this feature appears only at d_{Al} values significantly above those required to cause the ester modes to vanish. In principle, it is possible that newly formed molecular groups could be oriented in such a fortuitous way that the transition dipole moments of the oscillators are all parallel to the surface, thereby being inactive toward infrared excitation.[20] However, this situation is unlikely, since not all modes would be expected to have identical dipole orientations.

3.4. Secondary Ion Mass Spectrometry. Overall, the complete mass spectra of both positive and negative ions show that the starting monolayers are quite pure. As a background for discussing the effects of Al, we briefly review useful diagnostic peaks for the pure SAM. The relative intensities of Au_x and Au_xS_y cluster ions are in excellent agreement with those observed previously,[32−34] and no features were observed that indicate the presence of oxidized alkanethiolate species such as sulfonate.[32−35] The information associated with the positive ion spectra of the bare monolayers is found mostly below a mass-to-charge ratio (*m*/z) of 200. Prominent features of the **M-Au** spectra are characterized by the chemical formulas $(CH_2)_x^+$, $(CH_2)CH^+$, $CH_3(CH_2)_x^+$, and $S(CH_2)_x^+$. Prominent features in the **ME-Au** spectra are characterized by $(CH_2)_x^+$, $(CH_2)CH^+$, $S(CH_2)_x^+$, $(CH_2)_xCO^+$, and $(CH_2)_xCO_2CH_3^+$. The negative ion spectra of the bare **M-Au** and **ME-Au** monolayers exhibit a number of high-mass ions containing intact adsorbate molecules such as AuA^-, Au_2A^-, and AuA_2^-, where A is the adsorbate species, as well as Au_x^- and $Au_xS_y^-$ clusters. Other diagnostic ions of interest include $AuS(CH_2)_x^-$ in the **M-Au** spectrum and $AuS(CH_2)_x^-$ and $(CH_2)CO_2^-$ in the **ME-Au** spectrum.

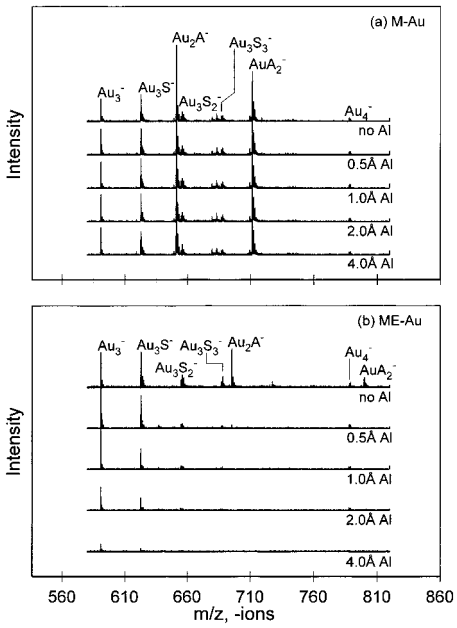

Figure 7. Negative SIMS spectra of methyl-terminated and methyl ester-terminated SAMs for different total Al doses. The symbol **A** in the mass fragment peaks represents the intact adsorbate species.

Following analysis of the bare monolayers, Al was deposited, and changes in intensity were tracked for the aforementioned ions as well as for new features in the mass spectra involving metal−organic ions. Figure 7 shows the $m/z = 580-820$ region of the negative ion mass spectra for **M-Au** and **ME-Au** at $d_{Al} = 0$, 0.5, 1.0, 2.0, and 4.0 Å. The spectra for both monolayer systems contain a series of peaks including Au_3^-, Au_3S^-, $Au_3S_2^-$, $Au_3S_3^-$, Au_4^-, Au_2A^-, and AuA_2^-.

The relation of Au_2A^- and AuA_2^- intensities to d_{Al} is shown in Figure 8. The plot for Al deposited onto **M-Au** (Figure 8a) shows that the intensity of ions involving the CH_3 functionality increases with the initial increment of deposition and then holds a constant intensity as further Al is deposited. The lack of an intensity drop indicates that the alkyl chains are not chemically modified by Al metal, consistent with the results of XPS and IRS experiments. The intensity increase presumably arises from the electropositive Al atoms, which act as an electron source for the more electronegative desorbing ions.[36] In contrast, for Al deposited onto **ME-Au** (Figure 8b), ions involving the $-CO_2CH_3$ functionality vanish by $d_{Al} = 1.0$ Å, an indication that one Al atom reacts per functional group. This result is consistent with data from both XPS and IRS, which each show that all functional groups have undergone chemical modification at this coverage. Evidence of the chemical interaction between Al and the $-CO_2CH_3$ group is revealed in Figure 9 by the appearance of the $[CO_2]Al^+$ and $[(CH_2)_3CO^-]Al$ ions and their increasing intensities relative to the initial intensities of $C_5H_{11}^+$ and $C_5H_5S^-$, respectively, as the deposition proceeds. The lack of multiple-metal complex peaks in the spectra is further evidence for the reaction of only one Al atom per $-CO_2CH_3$ group. Other metal−organic fragments of the form $AlOC(CH_2)_x^{\pm}$ and $AlO_2C(CH_2)_x^{\pm}$, as well as $AlOC^+$ and AlO^-, are observed. The lack of $Au_xAl_yS_z^-$, AlS_x^-, and $AlS(CH_2)_x^+$ ions for Al deposition onto **ME-Au** indicates that Al penetration to the SAM/Au

(32) Tarlov, M. J.; Newman, J. G. *Langmuir* **1992**, *8*, 1398−1405.
(33) Hagenhoff, B.; Benninghoven, A.; Spinke, J.; Liley, M.; Knoll, W. *Langmuir* **1993**, *9*, 1622−1624.
(34) Wood, M. C. Surface Characterization and Imaging with Ion-Induced Desorption and Multiphoton Resonance Ionization. Ph.D. Thesis, Penn State University, 1995; pp 34−111.
(35) Hutt, D. A.; Cooper, E.; Leggett, G. J. *J. Phys. Chem. B* **1998**, *102*, 174−184.
(36) Czanderna, A. W.; Hercules, D. M. *Ion Spectroscopies for Surface Analysis*; Plenum Press: New York, 1991; pp 45−141.

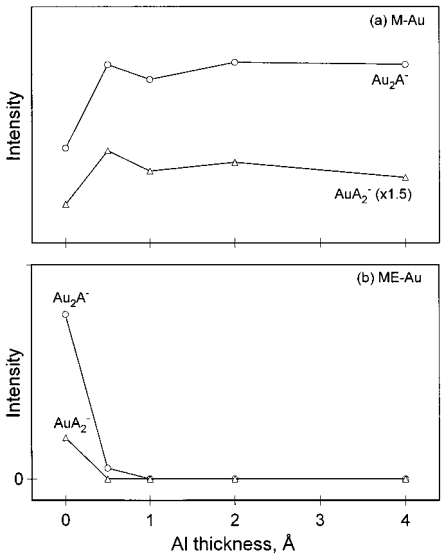

Figure 8. Plots of intensities of the Au_2A^- and Au_2A^- mass fragments for the methyl- and methyl ester-terminated SAMs versus total dose of deposited Al. The symbol **A** in the mass fragment peaks represents the intact adsorbate species. Under these conditions, the relative peak intensities were reproducible to ±6% for sample-to-sample and scan-to-scan on the same sample.

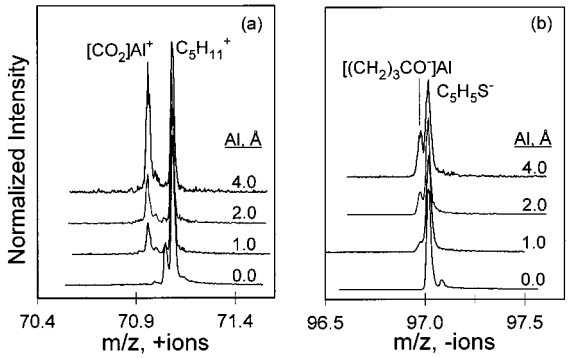

Figure 9. High-resolution ToF-SIMS spectra for methyl ester-terminated SAMs at different total Al doses.

interface does not occur. Formation of $Au_xAl_yS_z^+$ mass fragments is completely independent of distances over which that recombination can occur.

Cluster ions involving Al, S, and/or Au atoms are examined for evidence of diffusion of deposited Al to the SAM/Au interface region, as suggested above. As shown in Figure 10, Al deposited onto **M-Au** does result in the appearance of peaks indicating penetration of Al to the SAM/Au interface. This effect is made obvious in the observation of the increasing intensity of $AlSH_2^+$, $AlSCH_2CH^+$, $AuAlS^-$, and AlS_2^- relative to $C_2H_5S^+$, $C_6H_{14}^+$, and $[S_2C_{18}H_{35}]Au^{2-}$, respectively, as the deposition progresses. These spectra are normalized to the initial intensities of $C_2H_5S^+$, $C_6H_{14}^+$, and $[S_2C_{18}H_{35}]Au^{2-}$ to make obvious the increasing intensity of the metal−organic fragments relative to the organic fragments. The AlS_2^- mass fragment is normalized to the Au^- signal intensities. Absolute intensities decrease when $d_{Al} > 2.0$ Å due to the thickening Al overlayer. Other fragments of the form $Au_xAl_yS_z^-$ and $AlS(CH_2)_x^+$ also are observed.

One possible mechanism for the observed Al penetration involves the presence of static defects, viz. "pinholes", in the films where groups of alkanethiolate chains are missing. In this mechanism, the impinging vapor-deposited atoms could penetrate by being deposited directly into the open areas or by

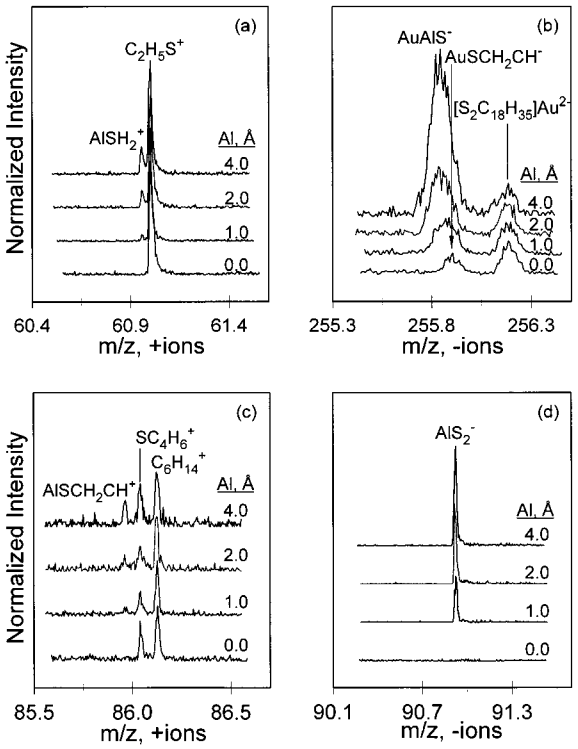

Figure 10. High-resolution ToF-SIMS spectra for methyl-terminated SAMs at different total Al doses.

preadsorbing onto dense regions of the SAM surface, followed by random surface diffusion to the open areas. Parallel experiments on companion samples show that the films are strongly electrochemically blocking.[37] This can be taken as evidence that the films are quite dense and relatively free of "pinhole" defects. Further, the ToF-SIMS and IR data suggest that Al has penetrated evenly across the Au−S interface, contrary to what would be expected for deposition into isolated defect regions.

The Al^+, Al_2^+, and Al_3^+ cluster peak intensities for **M-Au**, bare Au and **ME-Au** samples are given in Figure 11a−c, respectively, as a function of d_{Al}. The bare gold was cleaned of organic adsorbates by sequential immersion in 30% H_2O_2 and gas-phase UV−O_3 exposure. For both **M-Au** and bare Au (Figure 11a,b, respectively), the Al^+ and Al_2^+ intensities increase in parallel fashion up to $d_{Al} \approx 1$ Å, while the Al_3^+ does not. Above $d_{Al} \approx 2.0$ Å, all three cluster ions are observed, and the intensities increase with increasing Al coverage. The early appearance of the Al_2^+ peak indicates that the deposited Al atoms have already begun to cluster to some extent, as opposed to being localized as isolated atoms (greater than several diameters apart). Cluster ions are formed when component atoms at the surface are within ~5 Å of one another during the ion bombardment event.[38] The qualitatively similar behavior of **M-Au** and bare Au is interpreted as support for penetration of the Al atoms to the SAM/Au interface in the **M-Au** case. In contrast, for Al deposited onto **ME-Au** (Figure 11c), only Al^+ is observed for $d_{Al} < 1.0$ Å. Appreciable levels of Al_2^+ and Al_3^+ appear only when $d_{Al} > 1.0$ Å. These data indicate that, at low coverage, the Al overlayer on **ME-Au** consists primarily of isolated atoms bound to $-CO_2CH_3$ functional groups. The

(37) Porter, M. D.; Bright, T. B.; Allara, D. L.; Chidsey, C. E. D. *J. Am. Chem. Soc.* **1987**, *109*, 3359−3568.

(38) Winograd, N. *Mat. Fys. Medd. K. Dan. Vidensk. Selsk.* **1994**, *43*, 223−254. Liu, K. S.; Vickerman, J. C.; Garrison, B. J. In *Secondary Ion Mass Spectrometry SIMS XI*; Gillen, G., Lareau, R., Bennett, J., Stevie, F., Eds.; John Wiley & Sons: New York, 1998; p 443.

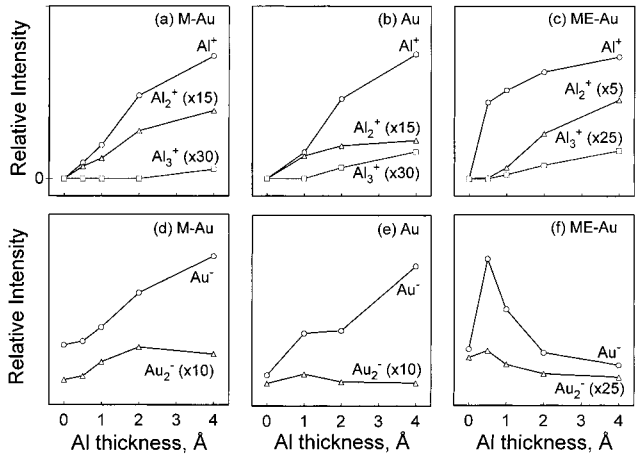

Figure 11. Plots of Al monomer, dimer and trimer peak intensities versus overlayer thickness. Plots a, b, and c show the Al_x^+ ion fragments from the methyl-terminated SAM, bare gold film, and methyl ester-terminated SAM, respectively. Plots d, e, and f show the Au_x^- ion fragments from a methyl-terminated SAM, bare gold film, and methyl ester-terminated SAM, respectively. Note the scale expansions on some of the plots.

appearance of Al_n^+ peaks is interpreted as an indication that additional Al initiates the formation of small islands.

The corresponding Au^- and Au_2^- spectra for the above samples are presented in Figure 11d,e. As the deposition progresses on bare Au, the ion yields increase. This effect is expected on the basis of an electron transfer from Al atoms to the more electronegative Au atoms during ejection from the surface. This trend is also observed for Al deposited onto **M-Au** (Figure 11d), further supporting the conclusion that Al atoms penetrate to the SAM/Au interface. Initial deposition of Al onto **ME-Au** also causes the Au ion intensity to increase in value, as shown in Figure 11f. However, in contrast to the other surfaces, the Au ion signals are quickly attenuated by $d_{Al} \approx 0.75$ Å. This result indicates that the ejection of substrate fragments is being blocked by formation of an overlayer at the vacuum interface.

3.5. Spectroscopic Ellipsometry. The spectra collected in real time during the first ~94 s of the Al deposition on **ME-Au** are shown in Figure 12. The data are plotted as a function of time (t) in terms of the real and imaginary parts of the pseudodielectric function, $\langle\epsilon\rangle = \langle\epsilon_1\rangle + i\langle\epsilon_2\rangle$, defined as

$$\langle\epsilon\rangle = \sin^2\theta\{1 + [(1-\rho)/(1+\rho)]^2 \tan^2\theta\}$$

In this equation, θ is the angle of incidence and $\rho = r_p/r_s$, where r_p and r_s are the complex Fresnel coefficients.[39] The pseudodielectric function is defined such that a single ideal interface between the ambient vacuum and a hypothetical material of dielectric function $\langle\epsilon\rangle$ gives the same (ψ, Δ) spectra as the complicated Al/**ME-Au** sample structure. The two three-dimensional surfaces in Figure 12 were constructed from 100 pairs of spectra, each having 83 photon-energy positions from 1.3 to 4.0 eV.

Two qualitative features are readily observed in the figure. First, along the $t = 0$ s line in the $\langle\epsilon_2\rangle$ spectrum, the feature near 2.5 eV is associated with the intrinsic d-band to Fermi level transitions of the Au.[40] Note that only after ~30 s of deposition does this feature change significantly. A later analysis shows that this represents the transition between the initial formation of an optically nonadsorbing dielectric layer on the monolayer surface and the subsequent formation of optically absorbing metallic Al particles. The continued visibility of the Au d-band transition with deposition shows that the Al film remains semitransparent throughout. The later analysis shows that the final Al film thickness is ~150 Å for the final spectra at $t \approx 94$ s. Second, both sets of spectra in Figure 12 show no evidence of the parallel-band feature at 1.5 eV that is dominant in the spectra of bulk Al.[41] As will be discussed in detail below, this observation can be attributed to a high film defect density that reduces the relaxation time of the excited electrons such that the bulk Al optical features are broadened beyond recognition.[42]

The spectra of Figure 12 were first analyzed for evidence of the formation of a dielectric overlayer caused by a chemical reduction of the initial Al flux by the terminal ester groups of the **ME-Au** monolayer. A preliminary least-squares regression analysis (LRA) was carried out using a two-layer optical model (ambient/dielectric layer/**ME-Au**), in which the optical properties of Al_2O_3 were assigned to the dielectric layer.[43] From this analysis, it was found that the Al atoms arriving during the first 28 s form a dielectric layer of thickness $d_{diel} = 6 \pm 1$ Å at the **ME-Au** surface, while further deposition results in unreacted Al(0). The use of any metallic-like properties for the initial layer ($t < 28$ s) gives quite poor fits to the data, whereas for the layer forming at later times, metallic properties must be included to obtain good fits.

The data from the preliminary analysis were applied as trial conditions for a more rigorous analysis using a three-layer model (ambient/Al/dielectric/**ME-Au**). In this procedure, based on a previous method,[44] values for d_{diel} and d_{metal}, as well as the spectra in $(\epsilon_1,\epsilon_2)_{metal}$, were deduced at different times during the deposition. In this analysis, as well, the optical properties of Al_2O_3 were assigned for the dielectric layer. The procedure was guided by the results of a previous study of Al deposition onto SiO_2/Si substrates,[45] in which the interaction between Al and SiO_2 has been well characterized.[46,47] First, using trial d_{diel}, d_{metal} values, the experimental (ψ, Δ) spectra were mathematically inverted to obtain a trial $(\epsilon_1,\epsilon_2)_{metal}$. The constraint was applied that $(\epsilon_1,\epsilon_2)_{metal}$ must be free of Au interband transition artifacts in the 2.5 eV region.

A typical set of simulation results is presented in Figure 13, where the experimental (ψ, Δ) spectra after 34.8 s of deposition have been modeled. The plot shows the trial $(\epsilon_1,\epsilon_2)_{metal}$ spectra (smoothed for clarity of presentation) for different d_{diel} and d_{metal} values, with $(\epsilon_1,\epsilon_2)_{metal}$ assigned as that of Al_2O_3 (as noted above). Given the constraints that the simulation must both obey causality (i.e., the Kramers−Kronig relationships between ϵ_1 and ϵ_2) and show no substrate-related artifacts, the best fit to the experimental spectra is obtained for $d_{diel} = 6$ Å and d_{metal}

(39) For example, see: Azzam, R. M. A.; Bashara, N. M. *Ellipsometry and Polarized Light*; North-Holland: Amsterdam, 1976.

(40) Aspnes, D. E.; Kinsbron, E.; Bacon, D. D. *Phys. Rev. B* **1980**, *21*, 3290−3299.

(41) Smith, D. Y.; Shiles, E.; Inokuti, M. In *Handbook of Optical Constants of Solids*; Palik, E. D., Ed; Academic Press: Orlando, FL, 1985; p 369.

(42) Nguyen, H. V.; An, I.; Collins, R. W. *Phys. Rev. Lett.* **1992**, *68*, 994−997.

(43) The analysis essentially consisted of minimizing the unbiased estimator of the mean square deviation σ between experimental and calculated (tan Ψ, cos Δ) spectra (Aspnes, D. E. *Proc. Soc. Photo-Opt. Instrum. Eng.* **1981**, *276*,181−195). The optical properties of Al_2O_3 were assumed for the dielectric layer, and the layer thickness is the single free parameter.

(44) Arwin, H.; Aspnes, D. E. *Thin Solid Films* **1984**, *113*, 101−113.

(45) Nguyen, H. V.; An, I.; Collins, R. W. *Phys. Rev. B* **1993**, *47*, 3947−3965.

(46) Brendel, R.; Hezel, R. *J. Appl. Phys.* **1992**, *71*, 4377−4381.

(47) Hetch, M. H.; Vasquez, R. P.; Grunthaner, F. J.; Zamani, N.; Maserjian, J. *J. Appl. Phys.* **1985**, *57*, 5256−5261.

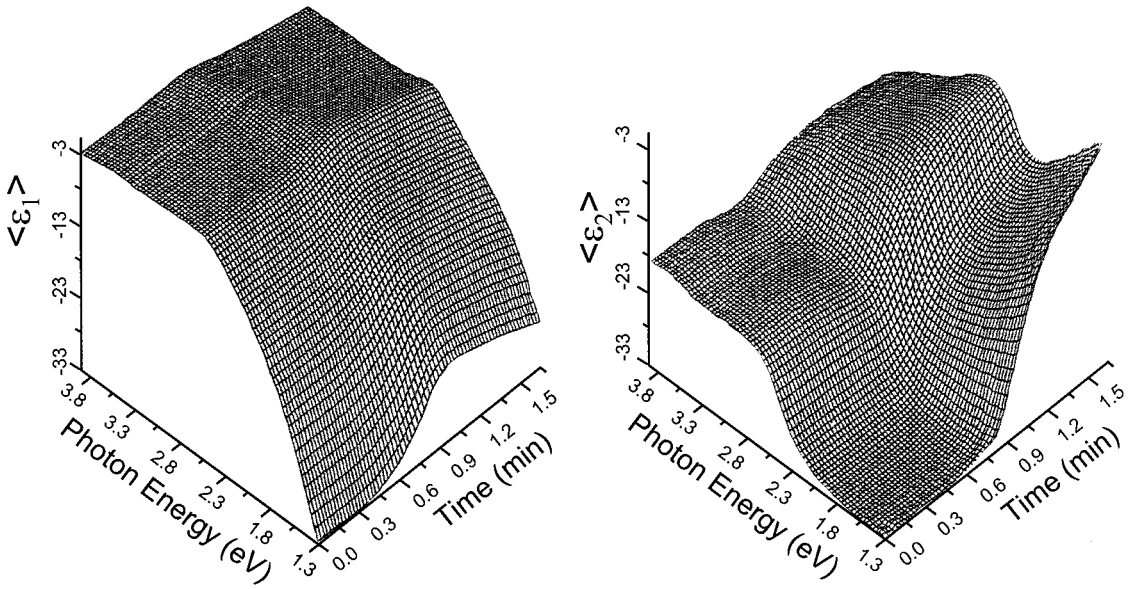

Figure 12. Real and imaginary parts of the pseudodielectric function collected in real time during Al evaporation onto a methyl ester-terminated SAM. A total of 100 pairs of spectra, each consisting of 83 spectral points, were collected over an Al deposition time of ~1.6 min (94 s). The aluminum deposition rate was initially slow and then accelerated after about 5 s. The total amount of Al deposited over the time scale of the plots is ~200 Å.

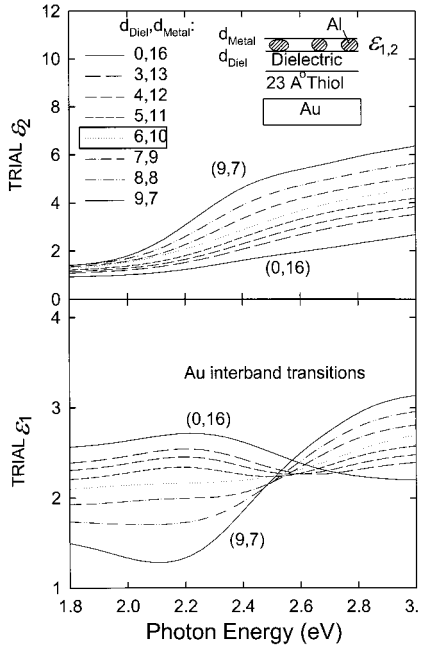

Figure 13. Trial dielectric functions for Al particle films determined from a three-layer model (ambient/Al/dielectric/**ME-Au**) of the real-time SE data collected at $t = 34.8$ s (see Figure 12). In obtaining these results, different choices of the dielectric and metallic Al film thicknesses, d_{diel} and d_{metal}, were made to allow mathematical inversion of (ψ, Δ) [or ($\langle\epsilon_1\rangle$,$\langle\epsilon_1\rangle$)]. The pair of correct thicknesses [(d_{diel}, d_{metal}) = (6 Å, 10 Å)] is the one that minimizes artifacts in the inverted dielectric function of the metallic Al particle film arising from structure in the substrate optical response. The data have been smoothed for clarity.

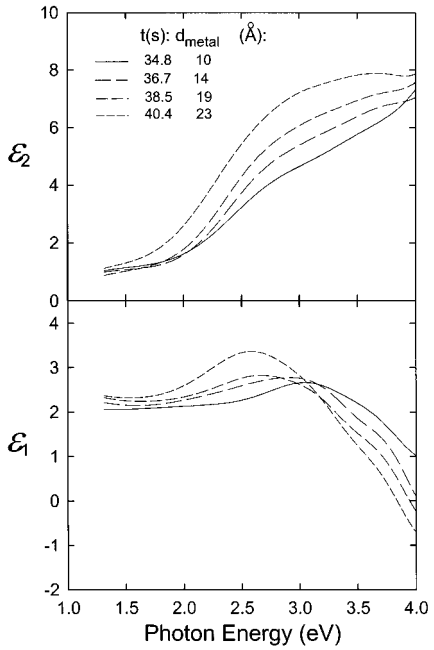

Figure 14. Selected metallic Al effective dielectric functions obtained from real-time observations of Al evaporation onto a methyl ester-terminated SAM. These results were calculated with the correct choice of the metallic Al thickness, d_{metal}, as determined from the analysis procedure of Figure 15. Here, the dielectric layer thickness at the SAM surface is assumed to be 6 Å.

= 10 Å. Note the agreement of d_{diel} with that from the preliminary LRA analysis at $t = 28$ s.

The above rigorous analysis was performed at different film growth stages from $t \approx 35$ to 42 s. The resulting best-fit $(\epsilon_1,\epsilon_2)_{metal}$ spectra of the evolving Al film are plotted for selected d_{metal} values in Figure 14. All the spectra exhibit shapes consistent with dominant dipolar plasmon adsorption features.[48] These features are uniquely characteristic of films consisting of isolated clusters of Al(0); they do not appear in nonmetallic states. The plasmon feature arises only in the experimental spectra taken after ~30 s of deposition, after which it is seen until full coalescence occurs. From this we conclude that the shift observed at ~30 s in the experimental spectra (Figure 12) is due to a change in the deposited film properties from a dielectric to a metallic type. Note that the plasmon band

(48) These features are similar to those observed for the Al/SiO_2 system, in which case isolated Al particles exhibit a single broad dipolar plasmon absorption feature in ϵ_2, peaking above 3.0 eV, along with normal (not anomalous) dispersion in ϵ_1 from 1.3 to >3.0 eV (Nguyen, H. V.; An, I.; Collins, R. W. *Phys. Rev. B* **1993**, *47*, 3947−3965.)

increases in magnitude and shifts to lower energies as the film thickness increases. The increase in magnitude is consistent with an increase in volume fraction of Al in the film. The shift to lower energy arises from local field effects in which the electric field within the Al clusters is screened by the dipole fields of neighboring clusters.

The trends in the Al dipolar plasmon band with increasing Al deposition can provide quantitative information on the changing morphology of the film. Following previous studies of Al/SiO_2,[45] the effective dielectric functions of Figure 14 were interpreted using a Maxwell−Garnett-type effective medium theory,[49] in which the parameters of interest can be deduced from a LRA. The two critical parameters related to film morphology are the Al volume fraction, Q, and the interparticle interaction parameter, F, which describes the screening effect.[45] Additional parameters are related to the parallel-band and free-electron (Drude limit) transition relaxation times, τ_{PB} and τ_D, which can be expressed in terms of a common electron mean free path, λ, describing the reduction of τ_{PB} and τ_D from their bulk value$_s$.[50]

The final results for Q and τ_{PB}, along with a summary of d_{diel} and d_{metal} values as a function of the deposition time, are shown in Figure 15. The bottom plot shows the onset of Al(0) at $t = 30$ s after the development of the 6-Å dielectric layer. In the gap between $t = 29$ and 32 s, there is insufficient Al in the metallic film (∼mass equivalent of 1 Å Al metal) for a two-layer analysis. For $t > 32$ s, the physical thickness of the Al film increases linearly with a deposition rate of 2.34 Å/s, as determined from the slope of the fitted dashed line. The relatively low Q values (middle plot) from ∼30 to 40 s of growth suggests that the Al(0) morphology consists of isolated clusters. The slow increase of Q from 0.12 to 0.21 with increasing time signals a trend toward coalescence of the clusters. The τ_{PB} values (top plot) remain nearly constant, at an average value of $\langle\tau_{PB}\rangle = 0.61 \times 10^{-15}$ s. This value is a factor of 7 smaller than the relaxation time for bulk Al ($\tau_{PB,b} = 4.1 \times 10^{-15}$ s;[41,45] horizontal solid line). The independence of τ_{PB} on thickness suggests that the electron lifetime is limited by scattering at internal defects within the clusters. Disorder and vacancies within the clusters, for example, may contribute to the enhanced scattering. The overall results for $t < 32$ s show that the Al(0) clusters do not form with bulk properties. This behavior is quite close to that observed for Al growth on SiO_2 under similar conditions.[45]

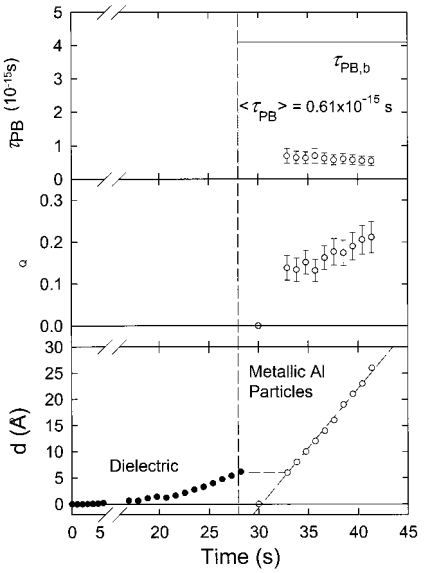

Figure 15. Summary of the parameters deduced in a complete least-squares regression analysis (LRA) of SE data obtained in real time during Al evaporation onto **ME-Au**. Top to bottom: the electron relaxation time, τ_{PB}, for the parallel-band transitions in the Al particles; the volume fraction of Al, Q; and the dielectric and metallic Al particle film thicknesses. The vertical line indicates the transition between the formation of a dielectric layer at the **ME-Au** surface and the formation of metallic particles (the latter at a physical thickness rate of 2.34 Å/s). The gap in the analysis between 29 and 32 s arises from the difficulty in interpreting the data for ultrathin metallic Al films. The Al particles exhibit an average parallel band relaxation time of 0.6×10^{-15} s, a factor of 7 lower than the bulk Al film value (horizontal solid line at top). Error bars on all parameter values are the 90% confidence limits in the LRA.

4. Discussion

4.1. Al Deposition on the CH_3-Terminated Monolayer. For convenience in following the discussion, the overall process of Al interaction with **M-Au** as a function of coverage is summarized in cartoon form in Figure 16 (top).

The combination of the XPS, IRS, and ToF-SIMS conclusively shows that the alkyl C−C and C−H bonds in the *n*-alkanethiolate monolayer are chemically inert to the deposited Al atoms. In particular, there is no evidence for the formation of aluminum carbides, consistent with a previous report.[8a] This behavior contrasts sharply with that of Ti, where there is a high reactivity with C−H bonds to form carbides.[11]

While the alkyl chains remain inert to the Al atoms at all stages of the deposition, in contrast, the XPS and ToF-SIMS data reveal that an Al−S interaction occurs in the initial stages up to $d_{Al} \approx 2$ Å. Evidence for this is seen by comparison with the data for the ME-SAM. In the **M-Au** system, one observes $Au_xAl_yS_z^+$ ions, while none are observed for **ME-Au**. For both films, gold clusters are observed, but only **M-Au** has sulfur-containing mass fragments. These data show that the Al atoms must penetrate into the Au−S interfacial region. Further, since the IRS data show that Al deposition causes negligible conformational changes in the highly organized monolayer, the Al−S interaction cannot take place by a massive disruption of the monolayer structure.[51] The surprisingly small perturbations of the alkyl chain structures indicate that the Al atoms must undercut the alkanethiolate layer in an extremely even manner laterally such as to support the uniform packing of the chains. We note that diffusion of metal atoms to the substrate interface in SAMs has been observed previously by others,[8,52] so a precedent exists.

(49) Yamaguchi, T.; Yoshida, S.; Kinbara, A. *J. Opt. Soc. Am.* **1974**, *64*, 1563−1568.

(50) In including the electron relaxation times in the model, one must be aware that the bulk dielectric function for Al consists of both intraband (Drude free electron ≡ D) and interband (parallel-band ≡ PB) contributions. The latter occurs in the neighborhood of the Brillouin zone surfaces parallel to the square (200) zone faces in the Al band structure and leads to a sharp absorption onset, evident in ϵ_2 for bulk Al at $2|U_{200}| = 1.5$ eV. Here, U_K is the Fourier coefficient of the effective crystal potential for the reciprocal lattice vector K that corresponds to the (200) zone faces. (For details of the relationships, see: Ashcroft, N. W.; Sturm, K. *Phys. Rev. B* **1971**, *3*, 1898−1910.] Because of the spectral breadth of the strong high-energy tail associated with the (200) contribution, our data reflect both the D and PB transitions, whose bulk relaxation times (τ_b) are different. Furthermore, the electron scattering at surfaces or internal defects perturbs the τ_b values. This problem can be handled by employing a classical size−effect relationship, $\tau_j = \tau_{j,b}^{+}(v_F/\lambda)$, to describe the scattering, where v_F is the Fermi velocity, 2.02×10^8 cm/s, λ is the electron mean free path, j = D or PB, and b represents the bulk state (Kreibig, U.; Fragstein, C. V. *Z. Phys.* **1969**, *224*, 307−323). In this relationship, the τ_j values are reduced from the corresponding $\tau_{j,b}$ ones by a common λ, thus reducing the number of free parameters in the LRA from two (τ_{PB}, τ_D) to one (λ). Applying the size−effect relationship, the expression for Al particle dielectric function as a sum of the two contributions and the Maxwell−Garnett-type effective medium theory, Q, F, and λ, can be deduced from a LRA of the dielectric functions of Figure 16.

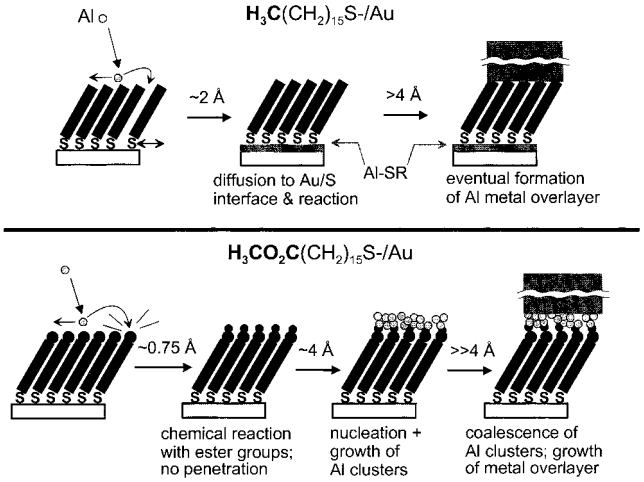

Figure 16. Cartoon illustration of important features of the Al interaction mechanisms with the methyl- and methyl ester-terminated SAMS. The top figure shows that, for the methyl-terminated SAM, the first ~2 Å of Al diffuses directly to the S/Au interface to form a smooth interlayer, while after ~4 Å a metallic overlayer at the SAM/vacuum interface forms. The bottom figure shows that, for the methyl ester-terminated SAM, the Al atoms react preferentially with the ester groups and do not diffuse to the S/Au interface. The first ~0.75 Å of Al is shown as forming a specific 1:1 reaction product with the terminal ester groups. After ~4 Å, metallic Al begins to nucleate in the form of discrete clusters, whereas at much larger thicknesses the Al forms a uniform metallic overlayer.

Since a perfectly ordered SAM would not have sufficient space between chains to allow penetration by Al atoms, the diffusion mechanism must involve defects. Two types can be considered: static and dynamic. Static defects include pinholes or patches of missing chains, disordered regions (e.g., in grain boundary regions of the Au{111} substrate), and line defects such as tilt-phase boundaries between domains of chains with opposite tilt angles. Since we observe that our self-assembly method produces SAMs that are highly blocking toward electrochemical processes,[37] our films are significantly free of pinhole defects. The most likely defects to allow Al entry are those in disordered regions surrounding {111} terraces. However, given that our data show a uniform lateral distribution of Al in the adlayer, entry via these defects would require a significant fraction of the nascent adatoms to diffuse considerable distances along the Au−S interfacial area in order to reach the central regions of the {111} terraces.

This difficulty is overcome through a dynamic mechanism involving channels formed by quasi-2-D, dynamic fluctuations of the surface positions of the alkanethiolate adsorbates.[53] Recent molecular dynamics simulations[54,55] of ordered alkanethiolate SAMs on Au(111) have shown that thermally induced, lateral fluctuations of the alkanethiolate lattice positions can occur at ambient temperatures to create transient, nanometer-scale open regions on the Au substrate. It is reasonable that diffusion could occur via these channels on the time scale between deposition and analysis (~minutes). The schematic in Figure 17 illustrates how the dynamic channel mechanism would work. The figure shows the alkanethiolate chains placed on a ($\sqrt{3} \times \sqrt{3}$), R30° Au(111) superlattice with the chain tilt vectors indicated on top of the adsorbates. The left figure shows a static overlayer, while the right shows one possible concerted fluctuation of R−S adsorbate positions on the Au surface, in which some of the S atoms move from a 3-fold hollow to an atop site on the Au(111) lattice. This transient defect contains a space sufficiently large to accommodate a 2.75-Å-diameter Al atom at the gold surface. Once at the S−Au interface, the Al atoms could either alloy with the Au[56] or chemically react with the S atoms. The latter possibility is supported by the observation of an Al 2p core-level peak in the region expected for Al_xS_y compounds. The simplest rationalization of this observation is that the Al atoms react with the thiolate S atoms to displace the Au and form Al alkanethiolate (Al−SR, where R = $C_{16}H_{33}$) adsorbate species. Such a reaction would be thermochemically driven by the much higher ionization potential of Al compared to that of Au.

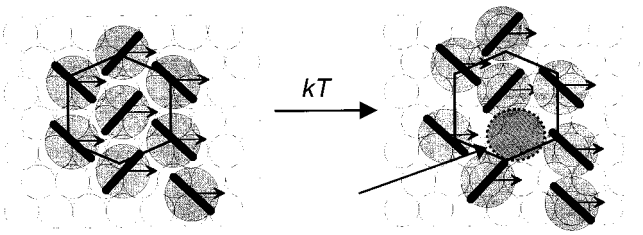

Figure 17. Schematic showing an underlying Au(111) terrace with an overlayer of an alkanethiolate, shown as large circles, on a $3^{1/2} \times 3^{1/2}$ R30° superlattice. The dark cylinders on the adsorbates indicate the top projection of the C−C−C direction, while the arrows indicate the chain axis tilt direction. The left-hand diagram shows a static lattice. The availability of thermal energy (*kT*) is shown as leading to a positional fluctuation in the right-hand diagram, where some adsorbates have shifted their S atoms from 3-fold hollows to atop sites on the Au lattice.

With increasing Al deposition up to $d_{Al} \approx 2$ Å, the XPS and ToF-SIMS data show that reactive penetration of Al continues. At increasing Al doses, however, both techniques indicate that this process stops in favor of formation of a metallic overlayer phase. One likely explanation is that formation of Al−SR bonds slows or stops the formation of quasi-2D transient defects and thus closes off the dynamic penetration channels. This behavior is reasonable on the basis that much higher barriers would be expected for lateral diffusion of RS species on an Al relative to a Au surface. At $d_{Al} \approx 2$ Å, ~12.1 Al atoms/nm^2 have been delivered to the sample. Based on the surface density of 4.6 molecules/nm^2 in an alkanethiolate SAM pinned at a ($3^{1/2} \times 3^{1/2}$) superlattice on a {111} surface,[10,57] there are ~12.1/4.6 = 2.6 Al atoms per S, far in excess of a 1:1 stoichiometry. Given the Au atom surface density of 13.7 atoms/nm^2, the limiting value of ~12.1 Al atoms/nm^2 may signal an approach to a 1:1 adlayer, consistent with formation of integral stoichiometry alloys in the Al/Au system.[56] The formation of a layered, organized SAM structure, **M**−**Al**(1 layer)−**Au**(bulk), is remi-

(51) An example of the latter is illustrated by the observation that penetration of H_2S and HCl vapor into densely packed alkanoic acid SAMs on Ag substrates interfaces results in chemical disruption of the SAM/Ag interface, with subsequent reorganization of the adsorbate molecules into discrete crystallites of bulklike material dispersed across the substrate surface (Tao, Y.-T.; Lin, W.-L.; Hietpas, G. D.; Allara, D. L. *J. Phys. Chem. B* **1997**, *101*, 9732−9740. Tao, Y.-T.; Hietpas, G. D.; Allara, D. L. *J. Am. Chem. Soc.* **1996**, *118*, 6724−6735).

(52) Jung, D. R.; Czanderna A. W.; Herdt, G. C. *J. Vac. Sci. Technol. A* **1996**, *14*, 1779−1787.

(53) Extensive consideration of such effects has been made in a study of O atom penetration into various Langmuir−Blodgett films by Naaman et al. (Paz, Y.; Trakhtenberg, S.; Naaman, R. *J. Phys. Chem.* **1994**, 13517−13523).

(54) Bhatia, R.; Garrison, B. J. *Langmuir* **1997**, *13*, 765−769.

(55) Bhatia, R.; Garrison, B. J. *Langmuir* **1997**, *13*, 4038−4043.

(56) A variety of Au/Al alloy compositions are possible (see: Murray, J. L.; Okamoto, H.; Massalaski, T. B. *Binary Alloy Phase Diagrams*; Okamoto, H., Subramanian, P., Kacprzak, L., Eds.; ASM International: New York, 1987; Vol. 1, p 122).

(57) Laibinis, P. E.; Whitesides, G. M.; Allara, D. L.; Tao, Y. T.; Parikh, A. N.; Nuzzo, R. G. *J. Am. Chem. Soc.* **1991**, *113*, 7152−7167.

niscent of the organized structures reported by Jennings and Laibinis, in which alkanethiols were chemisorbed directly onto electrochemically deposited Ag and Cu adlayers on Au substrates.[58]

4.2. Al Deposition on the $-CO_2CH_3$-Terminated Monolayer. The replacement of the terminal $-CH_3$ group by the $-CO_2CH_3$ group results in a completely different behavior upon Al deposition. The overall behavior we deduce from the data is summarized in Figure 16 (bottom).

All the characterization techniques provide evidence for the onset of a chemical reaction between Al and the $-CO_2CH_3$ group during the initial stages of Al deposition. While a chemical interaction is to be expected on the basis of previous work with polymer surfaces containing C═O groups,[12a−h] our data allow a detailed quantitative analysis due to the known density of surface functionality.

As a preliminary, we note that, as in the case of the **M-Au** system, there is no observed chemical reaction between Al and the alkyl chains of the SAM. Further, of primary importance, we note that there is no evidence for penetration into the **ME-Au** SAM. In particular, no diagnostic $AlSH_2^+$ or $AuAlS^-$ peaks are observed in the ToF-SIMS spectra.

It is clear for several reasons, however, that the Al reacts with the $-CO_2CH_3$ group. First, the XPS spectra show that the C 1s peaks for C═O and $-OCH_3$ vanish between $d_{Al} = 0.5-1.0$ Å. However, the continued observation of O 1s peaks indicates that the O atoms are still present, though apparently in a different oxidation state. The absence of any C 1s peaks in the aluminum carbide region indicates that the ester group does not suffer total reductive degradation.[59] Second, the ToF-SIMS spectra reveal that the adsorbate molecule mass fragments, Au_2A^- and AuA_2^-, vanish between $d_{Al} = 0.5$ and 1.0 Å, an indication that the parent molecules have been chemically converted to new forms. Finally, for $d_{Al} \approx 1.0$ Å, the IRS spectra show a loss of all modes related to the $-CO_2CH_3$ functional group, except for those associated with the CH_3 group. Since the latter modes are still observed, although somewhat diminished in intensity, one can conclude that the $-CO_2CH_3$ group is only perturbed, not completely degraded. The π character in the C═O bond appears to be completely missing since no characteristic spectral features appear at other typical frequencies, e.g., carboxylate modes between 1400 and 1650 cm^{-1}.

To facilitate quantitative interpretation of these data, we note that, at $d_{Al} = 0.76$ Å, the average surface density of Al atoms is 4.6 Al atoms/nm^2, equal to that of the alkanethiolate adsorbates (see calculations at the end of the previous section). Based on the above observations that initial reaction of all the ester groups is complete by $d_{Al} = 0.5-1.0$ Å, we conclude that the initial product has a 1:1 Al/ester stoichiometry. The complete loss of the π-bond character of the C═O bond, together with the continued presence of the O atoms and the CH_3 group, points to formation of an $Al-O-COCH_3$ species with sp^3 C atoms. In agreement with this picture, the SE data lead to the conclusion that the initial deposition of Al produces a dielectric layer, as opposed to metallic Al.

The XPS spectra reveal limited information on the electronic states of the atoms in the $Al-O-COCH_3$ complex. In the low-coverage samples, the unexpectedly higher binding energy of the Al 2p core-level peak (~75.2 eV), compared to that of aluminum oxide or sulfide, suggests that the fractional metal → ligand electron transfer in the complex is greater than that in the inorganic compounds.[60] This behavior also suggests the presence of the Al(III) state, since lower formal valence states would show Al 2p binding energies approaching the value of Al(0). The O 1s spectra show that, with 0.5−1.0 Å deposition of Al, the initial $-C{=}O$ and $-OCH_3$ peaks shift to slightly higher and significantly lower binding energies, respectively, to form a broad composite peak. This result shows that, in the complex, both O atoms have approached a similar electronic structure in which a significant degree of negative charge exists, such as in an oxide state. The C 1s core-level region indicates that the $C{=}O$ and $-OCH_3$ carbon atoms shift to an electronic structure similar to those in $-CH_2-$. A proposed structure for the complex, based on the above evidence, is shown below as **a**. The central C atom and the OCH_3 unit exhibit significant

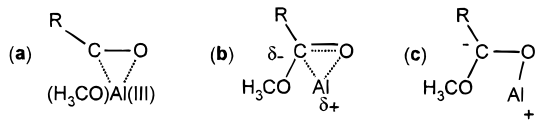

negative charge character, consistent with reduction of the C 1s binding energies for both C atoms. The reduction of the C═O bond order is consistent with the lowering of the O 1s binding energy of the associated O atom. The observation of the CH_3 mode IRS spectral features in similar positions before and after Al deposition points to the continued integrity of the CH_3 unit. Unfortunately, the easily observed CH_3 r^- mode frequency is not sensitive to whether the CH_3 is bonded to Al or O.[31] Other than a 1:1 Al:ester stoichiometry, the essence of structure **a** is distinctly different from that predicted from the calculations of Chakraborty, Davis, and Tirrell[14] for Al dimer interactions with a sequence of repeat units of poly(methyl methacrylate) (structure **c**). We have embodied our interpretation of their calculated features into structures **b** and **c**.[61] Structure **b** is an intermediate on the way to **c**, their lowest energy structure. In both cases, the incomplete transfer of the three electrons of Al to the organic moiety appears inconsistent with the high binding energies we observe for the Al 2p core-level XPS peaks. Recent density functional calculations have been performed by Travaly and co-workers on the aromatic ester group of poly(ethylene terephthalate).[62] Their calculations predict the most favorable interaction with one Al atom to be with the C═O group, to give a linear $Al-O-C$ complex. We note that they predict that introduction of additional Al atoms does not lead to reduction of the Al but rather to growth of the metallic phase, a distinct departure from our observations with the methyl ester group.

(58) Jennings, G. K.; Laibinis, P. E. *J. Am. Chem. Soc.* **1997**, *119*, 5208−5214.

(59) We note that an experimental study of the chemisorption of CH_3CO_2H onto bare Al surfaces at room temperature shows the formation of two species: a deprotonated acid attached to the Al by the two O atoms and a decomposition product with O−Al and C−Al species (Underhill, R.; Timsit, R. S. *J. Vac. Sci. Technol. A* **1992**, *10*, 2767−2774). While this result shows that Al(0) is capable of reducing a carbonyl group to carbide species at room temperature, it is clear in the present case that Al atoms deposited onto ester groups do not show this behavior.

(60) One must be cautious about such inferences. Literature values for core-level shifts in Al compounds have a wide range, typically ±1 eV (see refs 27 and 28), partly because the values come from spectra taken on bulk materials. Since the present case involves a very thin surface layer of Al−O−C species, it is possible that the formation of isolated, cluster-like surface species would cause the shift to 75 eV relative to ~74 eV observed for bulk aluminum oxide.

(61) In the work by Chakraborty, Davis, and Tirrell, a model was used in which pairs of Al atoms, spaced between neighboring $-CO_2CH_3$ units on a polymer sequence, were given the possibility of reacting with more than one $-CO_2CH_3$ group. The minimum potential energy structure obtained shows a single atom per functional group, a loss of C═O π bonding, and the presence of a negative charge on the central C and a positive charge on Al.

(62) Travaly, Y.; Bertrand, P.; Rignanese, G.-M.; Gonze, X. J. Adhesion **1998**, *66*, 339−355.

The effects of the formation of the Al−CO_2CH_3 complex on the IRS C−H stretching modes reveal something about the size of the complex. In particular, the positive frequency shifts show that the alkyl chains undergo significant conformational disordering (see Figure 5) upon Al interaction. The disorder presumably arises because of repulsive steric interactions between neighboring complexes at the chain termini. Since, on average, each terminus occupies an ∼5 Å diameter area at the surface [based on a ($3^{1/2} \times 3^{1/2}$) superlattice, see above], the Al−CO_2CH_3 complex size must exceed this value. Relief of steric interactions would occur with the introduction of gauche conformations, particularly near the chain termini, in concert with some untilting of the chains (more vertical orientations).

As the deposition proceeds beyond the ∼1 Å stage, the SE and XPS data indicate that a second stage of reduction of the surface groups occurs. The analysis of the SE data shows a best-fit model in which the Al is consumed initially to form an ∼6 Å overlayer film with dielectric properties, prior to the onset of metallic overlayer growth. Based on the XPS result that onset of the metallic Al 2p is not observed until after $d_{Al} \approx 4$ Å, we conclude that at least ∼3 Å of Al is involved in further reactions with the initial 1:1 Al−CO_2CH_3 complex. This amount of Al is equivalent to ∼4 Al atoms per ester. Since an aluminum carbide feature remains absent from the XPS and ToF-SIMS spectra (at all coverages) and the IRS spectra show the continued presence of the CH_3 group, the Al−CO_2CH_3 complex must retain some organic character and thus escapes ultimate degradation to inorganic oxide and carbide. Presumably, Al−Al bonds could be formed in the reduced complex.

Finally, after the completion of the ∼6 Å dielectric layer growth, both the XPS and SE data show that a metallic overlayer begins to form. The SE data are interpreted as revealing that the initial metal phase consists of small Al(0) clusters or droplets with a significant void content compared to bulk metallic Al. This behavior parallels that observed for deposition of Al onto purely oxide surfaces such as SiO_2. Finally, as the overlayer thickness approaches 30 Å, the morphology shows a trend toward uniform Al(0) film growth, which indicates that initial clustered metallic Al is beginning to coalesce. This is shown in Figure 15 (center), which shows that $Q \rightarrow 0.5$ as the film coalesces.

5. Conclusions and Future Work

This study shows that vapor-deposited Al atoms are unreactive with C−H bonds but shows an intermediate reactivity with the −CO_2CH_3 group to form organometallic products, as opposed to a high reactivity for which inorganic oxides and carbides would be formed.

For the **M-Au** SAM, the lack of a reactive terminal group combined with the dynamic positional fluctuations of the alkanethiolate overlayer allows penetration of the Al atoms into the SAM matrix and diffusion to the Au−S interface. The Al atoms form a uniform adlayer on the Au, with no disruption of the average chain conformational ordering and tilt angle. Once this interlayer is complete, Al penetration ceases, and metal overlayer growth initiates at the SAM−vacuum interface. This result indicates that the Al interlayer increases the pinning energies of the chain thiolate (RS−) headgroups and thereby quenches the dynamic fluctuation channel for Al penetration. Temperature-dependent studies should be quite useful in sorting out these phenomena,[53] and such studies are underway in our laboratories. The formation of such metallic interlayers will be of vital importance in the fabrication of molecular devices using metallized SAMs since device junction properties will vary strongly with the nature of the interlayer.[63]

The behavior of the **ME-Au** SAM contrasts sharply with that of **M-Au**. During all stages of the deposition, the Al atoms remain at the sample−vacuum interface. At the very early stages, Al atoms react with the ester groups to form a 1:1 Al: ester complex with a reduced C═O bond, an intact CH_3 group, and a sufficiently large size to cause partial conformational disordering of the chains. As deposition continues, this 1:1 complex undergoes further reaction with ∼4 atoms of Al per group. The structures of these species remain unclear, but the layer has no metallic character. Further addition of Al atoms results in the onset of nucleation of metallic clusters, with eventual coalescence above ∼30 Å of deposited metal. Associated studies of the electrical nature of these overlayers in the context of device contacts[63] are in progress.

These data illustrate how an organic functional group can serve as a chemical trap for diffusing metal atoms at a surface. There is strong precedent for this behavior, ranging from early work using thiol groups to control noble metal nucleation[64] to recent studies utilizing patterned functionality at surfaces as a template for CVD metallization.[3,4] Given the remarkable chemical and spatial variations possible with molecular surfaces, intriguing opportunities are suggested. For example, the use of phase-segregated films with nanometer-scale domains of groups such as CH_3 and CO_2CH_3[64] might lead to replicate patterns of overlayer organometallic compounds and metals. Another interesting possibility is the use of SAMs with interior functional groups, e.g., $HS(CH_2)_xCO_2(CH_2)_yCH_3$, to direct formation of a uniform metallic phase which grows outward from the interior of the SAM. Investigation of optimum combinations of metals and SAMs to provide such structures is underway in our laboratories.

Acknowledgment. The assistance of A. C. Miller in obtaining XPS data is greatly appreciated. Support from the National Science Foundation (A.E.H., D.L.A., R.W.C., N.W.), the Defense Advanced Research Project Agency (D.L.A.), and the Office of Naval Research (G.L.F., N.W.) is gratefully acknowledged.

JA9835234

(63) (a) Weiss, P. S.; Bumm, L. A.; Dunbar, T. D.; Burgin, T. P.; Tour, J. M.; Allara, D. L. *Ann. N. Y. Acad. Sci.* **1998**, *852*, 145−168. (b) Allara, D. L.; Dunbar, T. D.; Weiss, P. S.; Bumm, L. A.; Cygan, M. T.; Tour, J. M.; Burgin, T. P.; Jones, L. *Ann. N. Y. Acad. Sci.* **1998**, *852*, 349−370.

(64) Allara, D. L.; Hebard, A. F.; Padden, F. J.; Nuzzo, R. G.; Falcone, D. R., *J. Vac. Sci. Technol., A* **1983**, 376−382.

(65) Stranick, S. J.; Parikh, A. N.; Tao, Y. T.; Allara, D. L.; Weiss, P. S. *J. Phys. Chem.* **1994**, *98*, 7636−7645.